Measurement of the Ar($1s_y$) state densities by two OES methods in Ar–N_2 discharges

2014 Plasma Sources Sci. Technol. 23 015014

(http://iopscience.iop.org/0963-0252/23/1/015014)

IOP Publishing Plasma Sources Science and Technology

Plasma Sources Sci. Technol. **23** (2014) 015014 (9pp) doi:10.1088/0963-0252/23/1/015014

Measurement of the Ar($1s_y$) state densities by two OES methods in Ar–N_2 discharges

L M Isola, M López, J M Cruceño and B J Gómez

Instituto de Física Rosario (CONICET-UNR) 27 Febrero 210 Bis. (2000) Rosario, Argentina

E-mail: isola@ifir-conicet.gov.ar

Received 5 October 2013, revised 21 November 2013
Accepted for publication 25 November 2013
Published 4 February 2014

Abstract

In this work, results from two methods for the determination of the Ar($1s_y$) densities are compared in an Ar–N_2 discharge. These methods involve measurements of optical emission spectroscopy (OES). The first method (band method) uses the bands belonging to the $N_2(C \rightarrow B)$ second positive system, while the second method (branching fraction method) uses the line intensities corresponding to the Ar($2p_x \rightarrow 1s_y$) transitions. These techniques were tested in the negative glow of dc discharge and the results show remarkable agreement.

(Some figures may appear in colour only in the online journal)

1. Introduction

Plasmas generated in Ar–N_2 mixtures are the subject of considerable research due to the fact that they constitute the atmosphere present in many applications such as material treatment [1], film generation [2, 3], sterilization, plasma surgery, etc [4]. Optical emission spectroscopy (OES) is a non-intrusive and relatively easy-to-use procedure, which makes it widely applied to characterize Ar–N_2 plasmas for different pressure ranges, as well as for different discharge types and zones [5–10].

The argon metastable and resonant levels ($1s_y$ in Paschens notation) play an important role in discharge physics and chemistry [11]. Therefore, many direct measurement techniques were developed, such as laser absorption spectroscopy (LAS) [12–14], laser-induced fluorescence (LIF) [15, 16] and white-light absorption spectroscopy [17]. However, in these techniques, it is necessary to implement relatively complex experimental setups and procedures.

OES methods using line intensity ratios based on extended coronal models were implemented in [18–20]. However, these methods rely on the accuracy of the rate coefficient and *a priori* knowledge about the shape of the high-energy part of the electron energy distribution function (EEDF). Then, this kind of method is only applicable to specific discharge conditions.

Schulze *et al* [21] presented a robust method to determine the densities of the Ar($1s_y$) levels, which uses the change of the branching fraction of the Ar($2p_x \rightarrow 1s_y$) produced by photon reabsorption. The accuracy of the method was confirmed with the white-light absorption technique in [17] and with LAS in [11].

On the other hand, in the Ar–N_2 plasma, the high excitation transfer to N_2 from Ar($1s_y$) atoms produces a characteristic vibrational and rotational distribution in the $N_2(C)$ level [5, 22, 23]. In [24], a fit function of the second positive system (SPS) bands $N_2(\Pi\,^3C \rightarrow \Pi\,^3B)$ was proposed, which allows us to separate the excitation transfer contribution from that produced by collision with electrons. Hence, the knowledge of the $N_2(C)$ density populated by excitation transfer provides a way to measure the Ar($1s_y$) densities from the SPS bands.

In this paper, the Ar($1s_y$) density measurement method using the SPS band is compared with the branching fraction method (proposed in [21]) in dc N_2–Ar plasma. The advantages of these two methods are that they have a low number of theoretical assumptions (e.g. it is not necessary to know the EEDF shape) and they involve a relatively simple experimental setup; it is then possible to apply them to a wide variety of discharge conditions.

2. Theory

2.1. N_2 band method

The Ar addition in a N_2 discharge produces a strong change in the $N_2(C)$ rotational population due to the high excitation transfer to N_2 from Ar($1s_y$) atoms [23, 25]. So, it is possible to use this effect in order to calculate the Ar($1s_y$) densities from the measurements of an SPS band.

The $N_2(C)$ kinetic model is [24, 26].

(i) The main excitation reactions of state $N_2(C, v')$ are

$$e^- + N_2(X, v = 0) \rightarrow e^- + N_2(C, v') \quad \text{(a)}$$

$$N_2(X, v = 0) + Ar(1s_y) \rightarrow N_2(C, v') + Ar(^1S_0) \quad \text{(b)}$$

(a) The $N_2(C)$ level is primarily lost by radiative decay:

$$N_2(C, v') \rightarrow h\nu + N_2(B, v''). \quad \text{(c)}$$

The contribution of the *pooling* reaction, between two $N_2(A)$ metastable molecules, to the $N_2(C)$ population is negligible under our experimental conditions [24]. Then, this excitation process is not considered in the $N_2(C)$ kinetic model.

In [24], a fit function of the SPS bands was designed to separate the two population contributions to $N_2(C)$ (reactions (a) and (b)). This fit function uses two different rotational distributions, which take into account the characteristics of the excitation processes (a) and (b).

The fit function of the SPS band intensities is

$$\begin{aligned} I_{CB}(\lambda, \delta\lambda, \Delta\lambda, n_C^e, T_{rot}^x, n_C^{Ar^*}, T, \alpha, X) \\ = I_{CB}^e(\lambda, \delta\lambda, \Delta\lambda, n_C^e, T_{rot}^x) \\ + I_{CB}^{Ar^*}(\lambda, \delta\lambda, \Delta\lambda, n_C^{Ar^*}, T, \alpha, X) \end{aligned} \quad (1)$$

where $I_{CB}^e(\lambda, \delta\lambda, \Delta\lambda, n_C^e, T_{rot}^x)$ represents the part of the SPS bands populated by electron collision from the ground state, and it is given by

$$\begin{aligned} I_{CB}^e(\lambda, \delta\lambda, \Delta\lambda, n_C^e, T_{rot}^x) = \frac{K(\lambda) n_C^e(v') A_{CB}(v', v'') \tau_{v'}}{Q(T_{rot}^x)} \\ \times \sum_{i=P,R,Q} \sum_{\Omega=0,1,2} \sum_{J'} \exp\left(\frac{-B_X hcJ'(J'+1)}{k_B T_{rot}^x}\right) \\ \times \exp\left(\frac{-4\ln(2)\left[\lambda + \Delta\lambda - \lambda_\Omega^i(J')\right]^2}{(\delta\lambda)}\right) S_\Omega^i(J') \end{aligned} \quad (2)$$

where $K(\lambda)$ is the spectral response, $n_C^e(v')$ the population density of the upper level ($N_2(C, v')$) excited by electrons, $\tau_{v'}$ the lifetime of the v' vibrational level, $Q(T_{rot}^x)$ the partition function, $\delta\lambda$ the full-width at half-maximum of the rotational line, $\Delta\lambda$ a small shift in the wavelength which takes into account the small calibration error of the spectrometer [27], $A_{CB}(v', v'')$ is the Einstein coefficient [28], B_X is the rotational constant of the ground state, $S_\Omega^i(J')$ is the Hönl–London factor [29] and T_{rot}^x the rotational temperature of the ground state.

The second term of expression (1) represents the band part populated by excitation transfer from $Ar(1s_y)$ and it is given by

$$\begin{aligned} I_{CB}^{Ar^*}(\lambda, \delta\lambda, \Delta\lambda, n_C^{Ar^*}, T_{Ar^*}, \alpha, X) \\ = \frac{K(\lambda) n_C^{Ar^*}(v') A_{CB}(v', v'') \tau_{v'}}{Q(T_{Ar^*}, \alpha)} \\ \times \sum_{i=P,R,Q} \sum_{\Omega=0,1,2} \sum_{J'} \exp\left(-\left(\frac{B_X hcJ'(J'+1)}{k_B T_{Ar^*}}\right)^\alpha\right) \\ \times \exp\left(\frac{-4\ln(2)\left[\lambda + \Delta\lambda - \lambda_\Omega^i(J')\right]^2}{(\delta\lambda)}\right) S_\Omega^i(J') X(J') \end{aligned} \quad (3)$$

Table 1. Rate coefficients of the excitation transfer to $N_2(C, v' = 0, 1)$ and of the total excitation transfer to $N_2(C)$ from $Ar(1s_{3,5})$ reported in [31] (10^{-11} cm^{3}s^{-1}).

Levels	$\kappa_{Ar^*-N_2}^{v'=0}$	$\kappa_{Ar^*-N_2}^{v'=1}$	$\sum_{v'} \kappa_{Ar^*-N_2}^{v'}$
$Ar(1s_5)$	2.9 ± 0.3	0.75 ± 0.01	3.6 ± 0.4
$Ar(1s_3)$	0.6 ± 0.07	0.28 ± 0.05	1.4 ± 0.2

where $n_C^{Ar^*}(v')$ is the density in the $N_2(C)$ level populated by excitation transfer from $Ar(1s_y)$, $X(J')$ allows the alternation between even and odd K' rotational levels, and the rotational distribution is given by α and T_{Ar^*}. Naturally, when $\alpha = 1$, this rotational distribution is the Maxwell–Boltzmann distribution and T_{Ar^*} has the meaning of a rotational temperature.

Hence, $n_C^{Ar^*}(v')$ is calculated from the SPS band fit with expression (1). Then, $n_C^{Ar^*}(v')$ is a function of the $Ar(1s_y)$ density (see reaction (b)), as follows:

$$n_C^{Ar^*}(v') = n_{N_2(X)} \left(\sum_{y=2}^{5} n_{Ar(1s_y)} \kappa_{Ar(1s_y)-N_2}^{v'}\right) \tau_{v'}, \quad (4)$$

where $n_{N_2(X)}$ is the density of the $N_2(X)$ ground state, $n_{Ar(1s_y)}$ the $Ar(1s_y)$ density and $\kappa_{Ar(1s_y)-N_2}^{v'}$ is the rate coefficient corresponding to process (b).

Assuming that the excitation transfer (process (b)) is mainly produced from one of the $Ar(1s_y)$ states, equation (4) can be rewritten as

$$n_C^{Ar^*}(v') = n_{N_2(X)}\, n_{Ar^*}\, \kappa_{Ar^*-N_2}^{v'}\, \tau_{v'}, \quad (5)$$

where n_{Ar^*} is the density of the $Ar(1s_y)$ state that is responsible for the excitation transfer. Therefore, n_{Ar^*} can be calculated solving equation (5), as

$$n_{Ar^*} = \frac{n_C^{Ar^*}(v')}{n_{N_2(X)}\, k_{Ar^*-N_2}^{v'}\, \tau_{v'}}. \quad (6)$$

Two aspects are interesting to point out. The first is that in equation (6), n_{Ar^*} is calculated without the use of an $Ar(1s_y)$ kinetic model. The second is the assumption that the excitation transfer is mainly produced from only one of the $Ar(1s_y)$ states. The excitation transfer process to $N_2(C, v' = 0, 1)$ from $Ar(1s_5)$ is more efficient than the excitation transfer from $Ar(1s_3)$ (see table 1). In addition, it is expected that the $Ar(1s_5)$ population will be greater than the $Ar(1s_3)$ population (the statistical weight ratio for these levels is 5). On the other hand, the total rate coefficients of the excitation transfer to $N_2(C)$ from resonant levels is reported in [9]. The values are 1.6×10^{-11} cm^3 s^{-1} for $Ar(1s_2)$ and 3.6×10^{-11} cm^3 s^{-1} for $Ar(1s_4)$. However, in the literature, there are no reported values of the excitation transfer rate coefficients to $N_2(C, v' = 0, 1)$ (individual vibrational levels) from the $Ar(1s_2)$ and $Ar(1s_4)$ levels. So, it is difficult to weigh their contributions to these $N_2(C)$ vibrational levels. In [30], a qualitative discussion about the channels of energy transfer to $N_2(C, v' = 0)$ was performed through the time-dependent study of the SPS band intensity (with band head at 337.0 nm) in the afterglow of the Ar–N_2 discharge. The authors observed

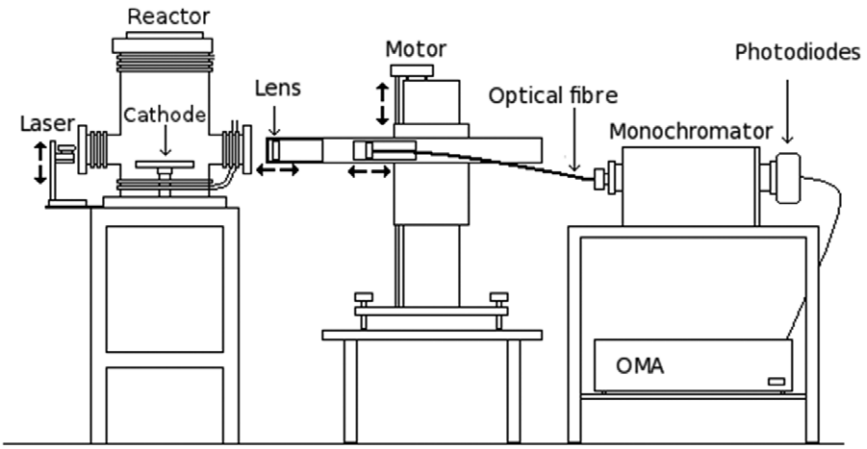

Figure 1. Experimental setup.

that the $N_2(C, v' = 0)$ population is a result of energy transfer mainly from the metastable states.

This analysis suggests that n_{Ar^*} calculated by the band method would be related to the $Ar(1s_5)$ density. This issue will be revisited in section 4.

2.2. Branching fraction method

In this section, the method to determine the $Ar(1s_y)$ densities using the change in the $Ar(2p_y \rightarrow 1s_y)$ branching fractions (due to the reabsorption process), developed in [21], will be presented.

When the emission produced by the transition from an upper level j to a lower level i is studied, it can happen that the lower level density was high enough so that the radiation reabsorption phenomena becomes preponderant. This will produce that the number of photons that arrives to the detector was less than expected, changing the branching fractions of the j level [17].

In order to quantify this reduction on the measured intensities, it is useful to work in the escape factor framework [32, 33]. So, the line intensity is

$$I_{j\rightarrow i} = K(\lambda)\, n_j\, A_{ji}\gamma_{ji}, \tag{7}$$

where n_j is the upper level density, γ_{ji} is the escape factor and $K(\lambda)$ is the spectral response, which becomes independent of λ after the intensity calibration. The exact evaluation of the escape factor is tedious and depends on quantities that are difficult to be evaluated, especially the spatial distribution of the upper and lower states. However, the analysis can be substantially simplified if a global approximation is used in the escape factor. This supposes a uniform spatial distribution of the density of the radiative and absorbent atoms. Mewe [33] developed the following approximation:

$$\gamma_{ji} = \frac{2 - \exp(-10^{-3}\, k_{ji}(\nu = \nu_{ji})\, l)}{1 + k_{ji}(\nu = \nu_{ji})\, l}, \tag{8}$$

where l is the characteristic scale length of the discharge and k_{ji} is the absorption coefficient. Equation (8) can be understood as all emitted photons escape when $k_{ji}\, l$ takes small values (thin target regime), while all photons are absorbed at large values of $k_{ji}\, l$. It is important to note that in the escape factor, the assumption of a uniform distribution of the density of the radiation and absorption atoms produces no significant errors, since the possible deviations tend to compensate [17].

The k_{ji} depends on the average lower level density $\overline{n_i}$ and it is defined as

$$k_{ji}(\nu = \nu_{ji}) = \frac{\lambda_{ji}^3}{8\pi^{\frac{3}{2}}} \sqrt{\frac{m}{2K_B T}}\, \overline{n_i}\, \frac{g_j}{g_i}\, A_{ij}. \tag{9}$$

Then, from equation (7) the intensity ratio between two lines produced by the transition from the same upper level j to the lower levels i and k is

$$\frac{I_{j\rightarrow i}}{I_{j\rightarrow k}} = \frac{\gamma_{ji}(n_i) A_{ji}}{\gamma_{jk}(n_k) A_{jk}}. \tag{10}$$

Then, it is clear that the intensity ratio only depends on the lower level densities n_i and n_k. Therefore, the lower level densities could be determined using different line intensity ratios. In order to decrease the calculation uncertainty, the least-squares method with many ratios has to be implemented. That is, to minimize the following expression:

$$\sum_j \sum_i \sum_k \left(\frac{I_{ji}}{I_{jk}} - \frac{\gamma_{ji}(n_{1s_i}) A_{ji}}{\gamma_{jk}(n_{1s_k}) A_{jk}} \right)^2. \tag{11}$$

3. Experiment

3.1. Experimental setup

The plasma reactor consists of a stainless steel chamber of 254 mm diameter and 360 mm height, with two side quartz windows (all the reactor dimensions are published in [34]). The discharge was generated between a central disc of 50 mm radius, which works as cathode, and the walls of the chamber (anode). The experimental setup is schematically shown in figure 1.

The focusing system consists of a quartz lens (150 mm focal length) and an optical fibre. The optical fibre is constructed by a bundle of silica-silica fibres (the individual

Table 2. Discharge current at different mixture gas concentrations. Pressure was 2.5 Torr and discharge voltage 500 V.

$[N_2]$ (%)	100	88	75	63	50	38
Current (A)	0.32	0.36	0.38	0.39	0.40	0.41
$[N_2]$ (%)	25	10	7	5	0	
Current (A)	0.41	0.41	0.41	0.43	0.56	

fibre diameter is 0.1 mm) with slit termination in one end. The lens is used to focus the plasma light in the circular entrance of the fibre. A laser was used to align the focusing system in order to collect the light of a selected area of the discharge.

A Jarrell-Ash monochromator with a Czerney–Turner mounting with an entrance slit of 25 μm and gratings of 1200 and 3600 lines mm^{-1} was used. A linear arrangement of 1024 photodiodes was used as a detector. Using the 1200 lines mm^{-1} grating, in the spectrum region of $\lambda = 750$ nm, the resolution is 0.06 nm pixel^{-1} with a resulting spectrum block of 60 nm measured at once. Relative intensity calibration of the spectra was performed using the known spectrum of a quartz tungsten halogen lamp.

The inflow was controlled by fine needle valves, which were previously calibrated to determine the gas mixture concentration.

In order to compare the two OES methods, the Ar($1s_y$) densities were measured at different distances from the cathode (z) and different gas mixture concentrations. In the experiments, the pressure was kept at 2.50 Torr and the total flow at 100 sccm. The plasma source was used in dc mode at 500 V.

In the measurements at different distances from the cathode, 6% N_2–94% Ar was used as plasma atmosphere. The discharge current was kept constant at 0.48 A.

On the other hand, the discharge current at different gas mixture concentrations is reported in table 2. In this study the spectra were measured focusing the plasma emission coming from the region at $z = 5$ mm.

3.2. Gas temperature measure

The two methods to measure the Ar($1s_y$) densities have the gas temperature as an input parameter. Since the $N_2^+(B)$ level is produced by electron collision from $N_2(X)$ ground state, the rotational distribution of the first negative system (FNS) bands corresponds to $N_2(X)$ rotational distribution [29]. Then, the ground state rotational temperature ($T_{\rm rot}^x$) can be calculated as the rotational temperature of the $I_{BX}^+(0–0)$ FNS band.

The rotational and vibrational constants reported in [28, 35, 36] were used in the fit function. Figure 2 shows the spectrum and its fit in a N_2–Ar discharge with a N_2 concentration of 50%. The gas temperatures at different gas mixture concentrations and different distances from the cathode are reported in tables 3 and 4, respectively.

In [27, 37], a function with a two-temperature Boltzmann rotational distribution was proposed to fit the FNS bands. However, the function with only one temperature Boltzmann rotational distribution produces a suitable fit on our FNS band spectra. This can be understood due to the fact that the main

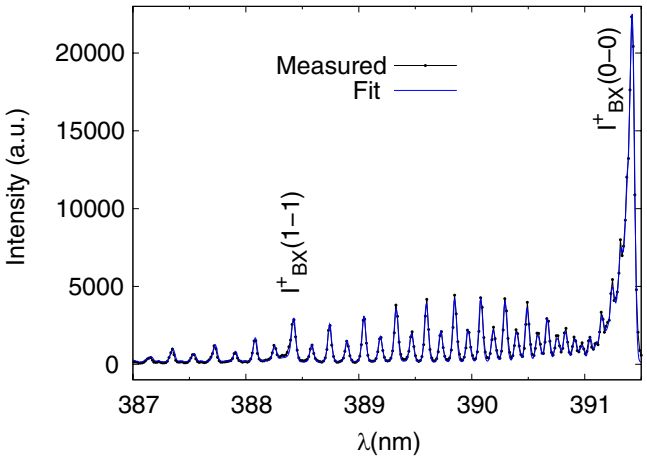

Figure 2. Measured and fitted $I_{BX}^+(0–0)$ FNS band at 50 N_2 concentration. Discharge conditions: 2.5 Torr, 500 V, 0.40 A and $z = 5$ mm.

Table 3. Gas temperature at different gas mixture concentrations.

$[N_2]$ (%)	100	88	75	63	50
$T_{\rm rot}^X$(K)	730 ± 20	760 ± 20	780 ± 20	780 ± 20	790 ± 20
$[N_2]$ (%)	38	25	10	7	5
$T_{\rm rot}^X$(K)	800 ± 20	800 ± 20	800 ± 20	810 ± 20	810 ± 30

excitation process to the $N_2^+(B)$ level is the electron collision. A large number of high-energy electrons, which are able to excite N_2 from the ground state to this level, is characteristic of the negative glow in a DC discharge [38, 39].

3.3. Band method

The values of $X(J')$, α and T were assessed fitting the spectrum measured in a discharge with small amount of N_2 ($\sim 0.5\%$) with expression (3), assuming that the process (b) is the only excitation mechanism under this condition. The estimated values are reported in table 5. The parameter uncertainties were estimated as the standard deviation in the least-squares method.

It is important to stress that the proposed rotational distribution for the $N_2(C, v' = 0)$ is in good agreement with the exhaustive measurements reported in [22]. This was discussed in greater detail in [24].

Figure 3 shows an emission spectrum measured from a 50% N_2 discharge. In this wavelength region it can be observed the $I_{CB}(0–2)$ and $I_{CB}(1–3)$ SPS bands with band head at 380.49 nm and 375.44 nm, respectively. The fit function (1) and its parts (2) and (3) are presented in the same figure.

Figure 4 shows the variation of the population process contributions as the N_2 concentration increases. It can be seen that only when the N_2 concentration is greater than 75%, the electron collision population process is dominant, while for lower N_2 concentrations the main population process is the excitation transfer from Ar($1s_y$). Moreover, the population of this vibrational level at 7% N_2 concentration is more than three times greater than in the N_2 discharge.

The normalized $n_{\rm Ar^*}$ was calculated from expression (6) using the $N_2(C)$ population density produced by excitation

Table 4. Gas temperature at different distances from the cathode.

z (mm)	2	3.5	5	7	9	11
T_{rot}^{X} (K)	890 ± 30	867 ± 30	860 ± 30	840 ± 30	810 ± 30	790 ± 30

Table 5. Fit parameters.

	$X(J')$	α	$T(K)$
$I_{BC}(0\text{–}2)$	1.19 ± 0.02	1.39 ± 0.06	3140 ± 60
$I_{BC}(1\text{–}3)$	1.19 ± 0.02	1.6 ± 0.2	2520 ± 90

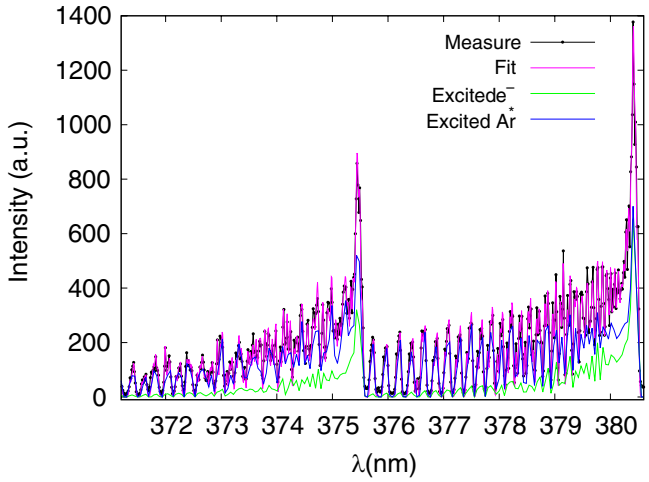

Figure 3. Measured $I_{CB}(0\text{–}2)$ and $I_{CB}(1\text{–}3)$ bands and fits at 50 N_2 concentration. Discharge conditions: 2.5 Torr, 500 V, 0.40 A and $z = 5$ mm.

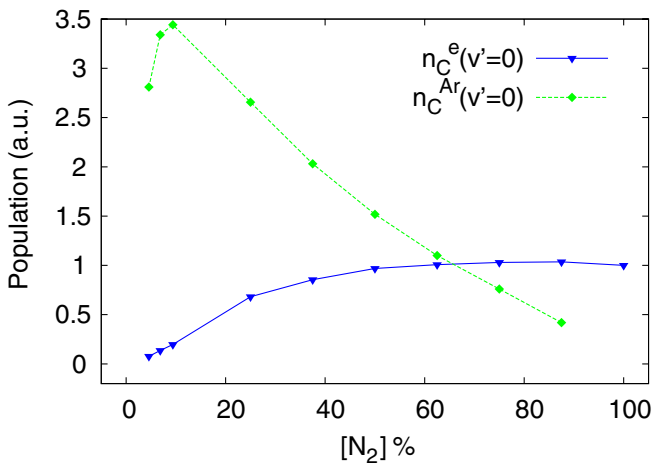

Figure 4. Population processes of $N_2(C, v' = 0)$. Discharge conditions: 2.5 Torr, 500 V and $z = 5$ mm.

transfer $n_C^{\text{Ar}^*}$, and it is shown in figures 5 and 6. Note that due to the relative calibration of the spectrum intensities, it is only possible to analyse the relative behaviour of the n_{Ar^*} density.

Figure 5 shows that n_{Ar^*} decreases rapidly between 6% and 23% of N_2. For higher N_2 concentrations the decrease is slower.

Figure 6 shows that n_{Ar^*} increases from the cathode up to $z = 3.5$ mm, and then decreases as the distance from cathode increases. The change in n_{Ar^*} at different distances

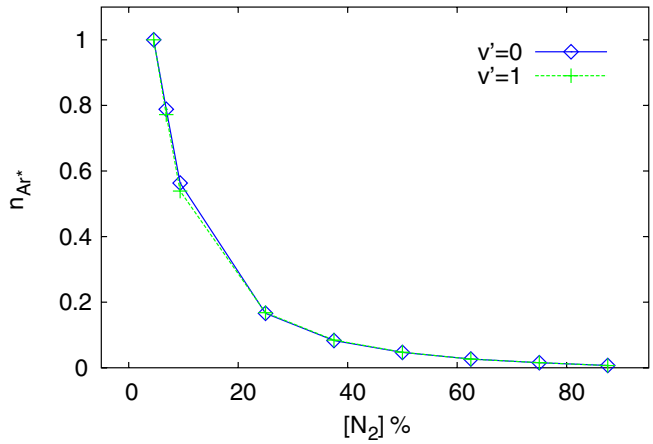

Figure 5. The normalized n_{Ar^*} as a function of N_2 concentration (5 mm): calculated from $n_C^{\text{Ar}^*}(v' = 0)$ ◊ and from $n_C^{\text{Ar}^*}(v' = 1)$ +. Discharge conditions: 2.5 Torr, 500 V and $z = 5$ mm.

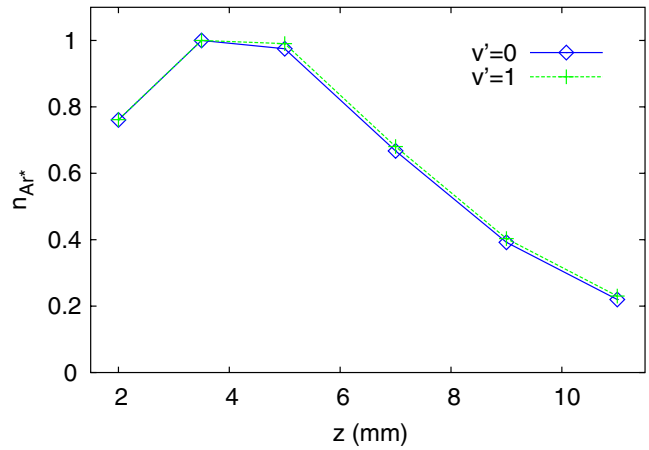

Figure 6. The normalized n_{Ar^*} at different distances from the cathode: calculated from $n_C^{\text{Ar}^*}(v' = 0)$ ◊ and from $n_C^{\text{Ar}^*}(v' = 1)$ +. Discharge conditions: 6% N_2–94% Ar, 2.5 Torr, 500 V and 0.48 A.

observed in this figure is the expected behaviour in this kind of discharge [40].

3.4. Branching fraction method

To measure the $\text{Ar}(1s_y)$ level densities, the emission produced by the $\text{Ar}(2p_x \rightarrow 1s_y)$ transition were used (see a spectrum in figure 7). Thus, the method developed in section 2.2 was implemented, using eight ratios: $2p_2 \rightarrow 1s_5 : 2p_2 \rightarrow 1s_2$, $2p_3 \rightarrow 1s_4 : 2p_3 \rightarrow 1s_2$, $2p_4 \rightarrow 1s_3 : 2p_4 \rightarrow 1s_2$, $2p_6 \rightarrow 1s_4 : 2p_6 \rightarrow 1s_2$, $2p_6 \rightarrow 1s_4 : 2p_6 \rightarrow 1s_5$, $2p_7 \rightarrow 1s_4 : 2p_7 \rightarrow 1s_3$, $2p_8 \rightarrow 1s_5 : 2p_8 \rightarrow 1s_4$ and $2p_{10} \rightarrow 1s_5 : 2p_{10} \rightarrow 1s_4$.

The scale length of the discharge was considered equal to the cathode radius ($l = 50$ mm), since the focusing system collects the emission from its centre. The $\text{Ar}(1s_y)$ densities as a function of the N_2 percentage are presented in figure 8.

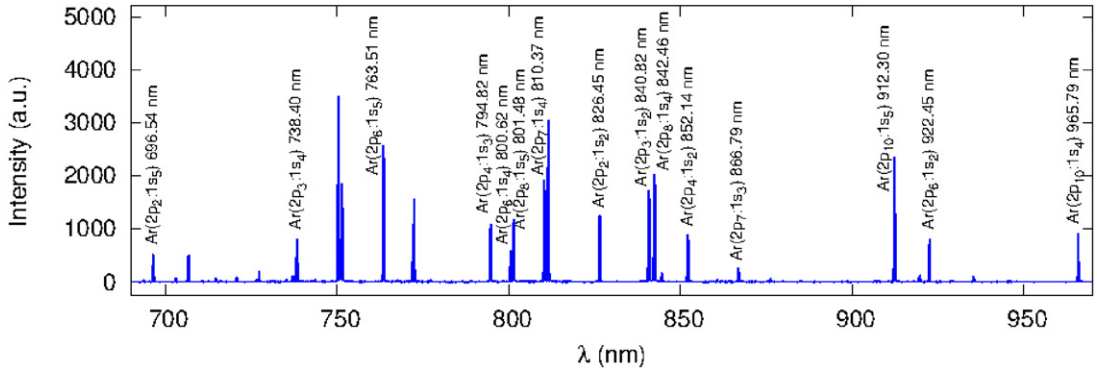

Figure 7. The Ar red line spectrum in an Ar discharge. Discharge conditions: 2.5 Torr, 500 V, 0.56 A and $z = 5$ mm.

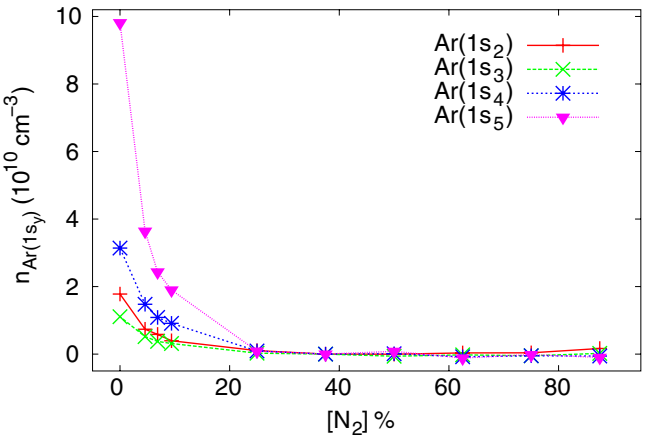

Figure 8. The Ar($1s_y$) density determined by the Ar branching fraction method. Discharge conditions: 2.5 Torr, 500 V and $z = 5$ mm.

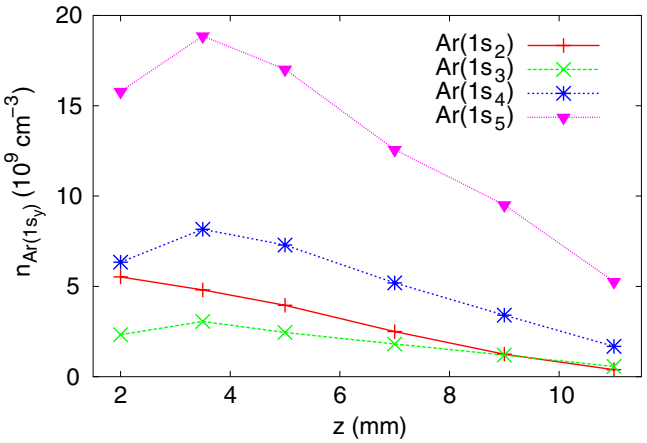

Figure 9. The Ar($1s_y$) density determined by Ar branching fraction method at different distances from the cathode. Discharge conditions: 6% N_2–94% Ar, 2.5 Torr, 500 V and 0.48 A.

The Ar($1s_y$) densities decrease rapidly when a small quantity of N_2 is added in the discharge. In Ar discharge, the density of the Ar($1s_5$) metastable state is almost three times greater than the other Ar($1s_y$) states. Note that this method returns very small values at N_2 concentration greater than 20%. This will be discussed in the following section.

The Ar($1s_y$) densities at different distances from the cathode are shown in figure 9. The four Ar($1s_y$) levels show similar behaviour; their densities increase from the cathode up to 3.5 mm and then decrease. These behaviours are very similar to that observed in figure 6.

4. Discussion

As it was noted in section 2.1, the metastable Ar($1s_5$) level could be mainly responsible for the excitation transfer process. So, in order to get a better understanding, it is interesting to compare the density of the Ar($1s_5$) level calculated through the Ar($2p_x \rightarrow 1s_y$) branching fraction method with n_{Ar^*} calculated by the SPS band method. These comparisons are presented in figures 10 and 11.

It is worth noting that the measurement of the Ar($1s_5$) density calculated by the branching fraction method at $z = 3.5$ mm and 6% of N_2 concentration was used to normalize the calculations of the SPS band method.

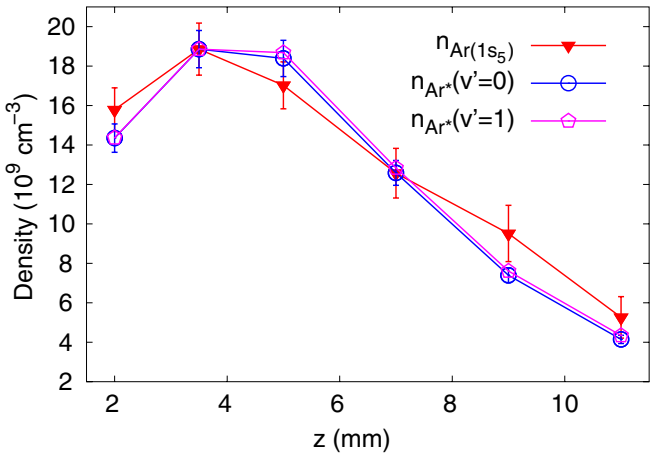

Figure 10. Ar($1s_5$) level population densities as a function of the distance from the cathode, calculated from the SPS band and the Ar($2p_x \rightarrow 1s_y$) branching fraction methods. Discharge conditions: 6% N_2–94% Ar, 2.5 Torr, 500 V and 0.48 A.

The good agreement between $n_{Ar(1s_5)}$ calculated by two methods at different distances from the cathode is remarkable (see figure 10). The uncertainties of $n_{Ar(1s_5)}$, calculated from the branching fraction method, were assessed considering the line intensity uncertainties, whereas, the band method uncertainties were propagated from the $n_C{}^{Ar^*}$ standard deviations recovered from the spectrum fit.

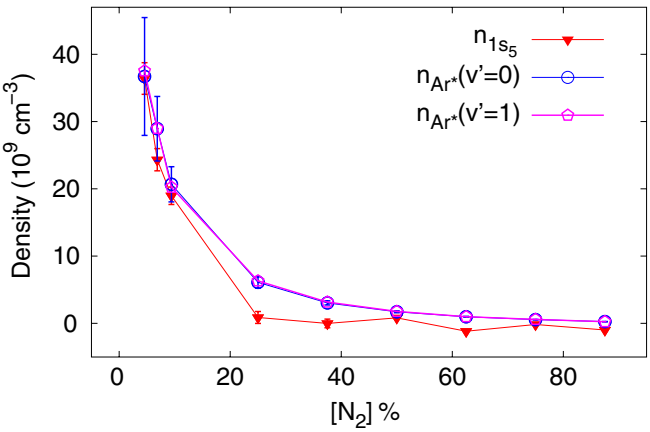

Figure 11. Ar(1s$_5$) level population densities as a function of the N_2 percentage, calculated from the SPS band and the Ar($2p_x \rightarrow 1s_y$) branching fraction methods. Discharge conditions: 2.5 Torr, 500 V and $z = 5$ mm.

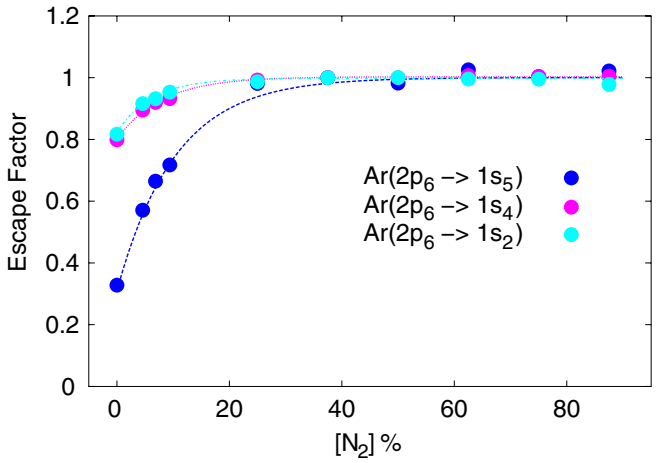

Figure 12. Escape factor of the three lines generated from the Ar(2p$_6$) state. Discharge conditions: 2.5 Torr, 500 V and $z = 5$ mm.

On the other hand, a good qualitative agreement between both calculation methods can be observed, when the gas mixture composition is changed (see figure 11). Both techniques show a strong decrease in the Ar($1s_y$) densities up to ~25% N_2 concentration. At higher N_2 concentrations, the decrease is less pronounced. The uncertainties were calculated in the same way as in figure 10. Nevertheless, in this case, it is necessary to take into account the n_{Ar^*} uncertainty produced by the $n_{N_2(X)}$ uncertainty (see equation (6)). This fact yields a large uncertainty at low concentrations of N_2 in the band method.

The low sensitivity of the branching fraction method at N_2 concentrations greater than 20% is produced by the low contribution of the photon reabsorption process. Figure 12 shows the escape factors of three lines as the N_2 concentration increases. The escape factor at N_2 concentration greater than 20% is near to 1. This means that each photon produced by the Ar($2p_x \rightarrow 1s_y$) transitions escapes without reabsorption. Therefore, the branching fraction method does not work at N_2 concentrations greater than 20%.

The concordance between the two methods suggests that the excitation transfer to $N_2(C, v = 0, 1)$ is mainly produced from Ar(1s$_5$). This agrees with the observation reported in work [30]. In figure 8, it can be observed that the Ar(1s$_5$) level has the largest population at N_2 concentrations lower than 20%. This fact explains that the excitation transfer from Ar(1s$_5$) was the main process to excite the $N_2(C, v' = 0, 1)$ levels. However, this reasoning may not be applied at N_2 concentrations greater than 20%. As was noted, the branching fraction method has low sensitivity to measure $n_{Ar(1s_y)}$ under these conditions. In addition, there is no report on the excitation transfer rate coefficients from the Ar(1s$_4$) level to the $N_2(C, v' = 0, 1)$ levels in order to weigh its contribution. Then, under these conditions, it is not possible to neglect the excitation transfer from the Ar(1s$_4$) level to the $N_2(C, v' = 0, 1)$ levels. So, n_{Ar^*} could reflect a mixture of the excitation transfer contributions from Ar(1s$_5$) and Ar(1s$_4$).

The knowledge of the SPS band rotational distribution produced by excitation transfer from the Ar(1s$_4$) level would lead to another way to separate the contribution of these levels. This would allow us to improve the fit expression (1) and to obtain both densities as a result. However, there is no measurement of this rotational distribution in the literature.

Summarizing, the branching fraction method allows us to calculate absolute densities for metastable and resonant Ar($1s_y$) states. The band method is useful, because of its greater sensitivity, especially for low Ar concentrations. Moreover, the band method uses only one spectrum, so it is useful when the discharge conditions change rapidly. Conversely, the branching fraction method involves the spectrum measurements in a long wavelength range.

5. Conclusions

Two OES methods to measure the Ar($1s_y$) densities were developed. The first uses the N_2 SPS bands and the second employs the Ar($2p_x \rightarrow 1s_y$) lines. These methods have the advantages of the low number of theoretical assumptions and a very simple experimental setup. This makes them very useful for a wide variety of discharge conditions.

These methods were tested in an Ar–N_2 dc discharge, when the gas mixture concentration was changed and at different distances from the cathode. The agreement between the two methods was remarkable.

The branching fraction method allows us to calculate absolute densities of the metastable and resonant Ar($1s_y$) states. Nevertheless, it involves the spectrum measurements in a long wavelength range.

The band method has greater sensitivity at low Ar concentrations, and the assessment is performed in one spectrum. As a result this is useful to study rapid changes under the plasma conditions.

Acknowledgments

The authors would like to thank Dr John Boffard and Dr Volker Linss for their time, generous dedication and enlightened discussions. We would also like to give acknowledgement

to CONICET (Argentina) and to the 'Agencia Nacional de Promoción Científica y Tecnológica' (National Agency for Scientific and Technologic Promotion), Argentina, PICT 12-01981/2008-0374 and Josefina Prats Fundation.

References

[1] Malvos H, Michel H and Ricard A 1994 Correlations between active species density and iron nitride layer growth in Ar–N_2–H_2 microwave post-discharges *J. Phys. D: Appl. Phys.* **27** 1328

[2] Borah S M, Bailung H, Pal A R and Chutia J 2008 Study on the influence of nitrogen on titanium nitride in a dc post magnetron sputtering plasma system *J. Phys. D: Appl. Phys.* **41** 195205

[3] Duquenne C, Tessier P Y, Besland M P, Angleraud B, Jouan P Y, Aubry R, Delage S and Djouadi M A 2008 Impact of magnetron configuration on plasma and film properties of sputtered aluminum nitride thin films *J. Appl. Phys.* **104** 063301

[4] Belostotskiy S G, Ouk T, Donnelly V M, Economou D J and Sadeghi N 2010 Gas temperature and electron density profiles in an argon dc microdischarge measured by optical emission spectroscopy *J. Appl. Phys.* **107** 053305

[5] Wang Q, Doll F, Donnelly V M, Economou D J, Sadeghi N and Franz G F 2007 Experimental and theorical study of the effect of gas flow on gas temperature in atmospheric pressure microplasma *J. Phys. D: Appl. Phys.* **40** 4202–11

[6] Debal F, Bretagne J, Jumet M, Wautelet M, Dauchot J P and Hecq M 2001 On the role of plasma-surface interactions in dc magnetron discharges in Ar–N_2 gas mixtures *Plasma Sources Sci. Technol.* **10** 30–7

[7] Annušová A, Foissac C, Krištof J, Veis P and Supiot P 2012 Spectroscopic diagnostics and modelling of a N_2–Ar mixture discharge created by an RF helical coupling device: II. Vibrational distribution of the $N_2(C\,^3\Pi_u, v')$ state *Plasma Sources Sci. Technol.* **21** 055022

[8] Henriques J, Taratova E, Dias F M and Ferreira C M 2002 Wave driven N_2–Ar discharge: II. Experiment and comparison with theory *J. Appl. Phys.* **91** 5632–9

[9] Kang N, Gaboriau F, Oh S and Ricard A 2011 Modeling and experimental study of molecular nitrogen dissociation in an Ar–N_2 ICP discharge *Plasma Sources Sci. Technol.* **20** 045015

[10] Britun N, Palmucci M, Konstantinidis S, Gaillard M and Snyders R 2013 Time-resolved temperature study in a high-power impulse magnetron sputtering discharge *J. Appl. Phys.* **114** 013301

[11] Li J, Liu F, Zhu X and Pu Y 2011 The spatially resolved measurements of the atomic densities in argon Paschen 1s levels by OES in a capacitively coupled plasma *J. Phys. D: Appl. Phys.* **44** 292001

[12] Belostotskiy S G, Ouk T, Donnelly V M, Economou D J and Sadeghi N 2011 Time- and space-resolved measurements of $Ar(1s_5)$ metastable density in a microplasma using diode laser absorption spectroscopy *J. Phys. D: Appl. Phys.* **44** 145202

[13] Vitelaru C, Lundin D, Stancu G D, Brenning N, Bretagne J and Minea T 2012 Argon metastables in HiPIMS: time-resolved tunable diode-laser diagnostics *Plasma Sources Sci. Technol.* **21** 025010

[14] Hubner S, Sadeghi N, Carbone E A D and van der Mullen J J A M 2013 Density of atoms in $Ar^*(3p^5 4s)$ states and gas temperatures in an argon surfatron plasma measured by tunable laser spectroscopy *J. Appl. Phys.* **113** 143306

[15] Macko P and Sadeghi N 2004 Determination of the non-relaxation (reflection) probability of metastable $Ar(^3P_2)$ atoms on a Pyrex surface *Plasma Sources Sci. Technol.* **13** 303

[16] Nafarizal N, Takada N and Sasaki K 2008 Production of ar metastable atoms in the late afterglow of pulse-modulated rf magnetron sputtering plasmas *J. Phys. D: Appl. Phys.* **41** 035206

[17] Boffard J B, Jung R O, Lin C C and Wendt A E 2009 Measurement of metastable and resonance level densities in rare-gas plasmas by optical emission spectroscopy *Plasma Sources Sci. Technol.* **18** 035017

[18] Vlcek J and Pelikán V 1989 A collisional-radiative model applicable to argon dischrages over a wide range of conditions: II. Application to low-pressure, hollow-cathode arc and low-pressure glow discharge *J. Phys. D: Appl. Phys.* **22** 632–43

[19] Boffard J B, Lin C C and DeJoseph C A Jr 2004 Application of excitation cross sections to optical plasma diagnostics *J. Phys. D: Appl. Phys.* **37** R143–61

[20] Li J, Liu F, Zhu X and Pu Y 2011 Determination of the metastable level densities in a low-pressure inductively coupled argon plasma by the line-ratio method of optical emission spectroscopy *J. Phys. D: Appl. Phys.* **44** 285203

[21] Schulze M, Yanguas-Gil A, von Keudell A and Awakowicz P 2008 A robust method to measure metastable and resonant state densities from emission spectra in argon and argon-diluted low pressure plasmas *J. Phys. D: Appl. Phys.* **41** 065206

[22] Nguyen T D and Sadeghi N 1983 Rotational and vibrational distribution of $N_2(C\,^3\Pi_u)$ excitation by state-selected $Ar(^3P_2)$ and $Ar(^3P_0)$ metastable atoms *Chem. Phys.* **79** 41–55

[23] Setser D W and Stedman D H 1970 Chemical applications of metastable argon atom: IV. Excitation and relaxation of triplet state of N_2 *J. Chem. Phys.* **53** 1004–20

[24] Isola L M, Lopez M and Gómez B J 2011 Study of the excitation mechanisms of the second positive system in the negative glow of a N_2–Ar discharge *J. Phys. D: Appl. Phys.* **43** 375204

[25] Derouard J, Nguyen T D and Sadeghi N 1980 Symmetries, propensity rules, and alternation intensity in the rotational spectrum of $N_2(C\,^3\Pi_u)$ excited by metastables $Ar(P_{0,2})$ *J. Chem. Phys.* **12** 6698–705

[26] Isola L 2012 Caracterización del brillo negativo de plasmas de N_2, Ar *y* N_2–Ar, mediante OES y sonda Langmuir *PhD Thesis* Universidad Nacional de Rosario, Facultad de Ciencias Exactas, Ingeniería y Agrimensura

[27] Linss V, Kupfer H, Peter S and Richter F 2004 Two $N_2^+(B\,^2\Sigma_u^+)$ populations with different Boltzmann distribution of the rotational levels found in different types of N_2/Ar discharges improved estimation of the neutral gas temperature *J. Phys. D: Appl. Phys.* **37** 1935–44

[28] Gilmore F R, Laher R R and Espy P J 1992 Frack-Condon fators, r-centroids, electronics transition moments, and Einstein coeficient for many nitrogen and oxigen band systems *J. Phys. Chem. Ref. Data* **21** 1005–107

[29] Hartmann G and Johnson P C 1978 Measurements of relative transition probabilities and the variation of the electronic transition moment for $N_2C\,^3\Pi_u$–$B\,^3\Pi_g$ second positive system *J. Phys. B: At. Mol. Phys.* **9** 1597–612

[30] Krylov B, Morozov A, Gerasimov G, Arnesen A, Hallin R and Heijkenskjöd F 2002 Channels of energy transfer to atomic nitrogen in excited argon-nitrogen mixtures *J. Phys. B: At. Mol. Opt. Phys.* **35** 4257

[31] Sadeghi N, Cheaib M and Setsers D W 1989 Comparison of the $Ar(^3P_2)$ and $Ar(^3P_0)$ reactions with chlorine and fluorine containing molecules: Propensity for ion-core conservation *J. Chem. Phys.* **90** 219–31

[32] Irons F E 1979 The escape factor in plasma spectroscopy: I. The escape factor defined and evaluated *J. Quant. Spectrosc. Radiat. Transfer.* **22** 1–20
[33] Mewe R 1967 Relative intensity of helium spectral lines as a function of electron temperature and density *Br. J. Appl. Phys.* **18** 107
[34] Isola L M, Gómez B J and Guerra V 2010 Determination of the electron temperature and density in the negative glow of a nitrogen pulsed discharge using optical emission spectroscopy *J. Phys. D: Appl. Phys.* **43** 015202
[35] Laher R R and Gilmore F R 1991 Improved fits for the vibrational and rotational constants of many state of nitrogen and oxigen *J. Phys. Chem. Ref. Data* **20** 685–712
[36] Gardet G, Moulard G, Courbon M, Rogemond F and M Druetta 2000 Evaluation of the rotational temperature in N_2 discharges using low-resolution spectroscopy *Meas. Sci. Technol.* **11** 333–41
[37] Linss V, Kupfer H, Peter S and Richter F 2005 Determination of the neutral gas temperature of nitrogen-containing low-pressure plasmas using a two-temperature model *Surf. Coat. Technol.* **200** 1696–701
[38] Kortshagen U and Tsendin L D 2002 *Electron Kinetics and Applications of Glow Discharges* (St.-Petersburg: Kluwer)
[39] Tsendin L D 2009 Electron kinetics in glows—from langmuir to the present *Plasma Sources Sci. Technol.* **18** 014020
[40] Bogaerts A 1999 Comprehensive modelling network for dc glow discharge in argon *Plasma Sources Sci. Technol.* **8** 210–29